

Dependences of the van der Waals atom-wall interaction on atomic and material properties

A. O. Caride, G. L. Klimchitskaya,^{*} V. M. Mostepanenko,[†] and S. I. Zanette

Centro Brasileiro de Pesquisas Físicas, Rua Dr. Xavier Sigaud, 150,

URCA, 22290-180, Rio de Janeiro, RJ, Brazil

Abstract

The 1%-accurate calculations of the van der Waals interaction between an atom and a cavity wall are performed in the separation region from 3 nm to 150 nm. The cases of metastable He^{*} and Na atoms near the metal, semiconductor or dielectric walls are considered. Different approximations to the description of wall material and atomic dynamic polarizability are carefully compared. The smooth transition to the Casimir-Polder interaction is verified. It is shown that to obtain accurate results for the atom-wall van der Waals interaction at shortest separations with an error less than 1% one should use the complete optical tabulated data for the complex refraction index of the wall material and the accurate dynamic polarizability of an atom. The obtained results may be useful for the theoretical interpretation of recent experiments on quantum reflection and Bose-Einstein condensation of ultracold atoms on or near surfaces of different nature.

PACS numbers: 34.50.Dy, 12.20.Ds, 11.10.Ws, 34.20.Cf

^{*} On leave from North-West Technical University, St.Petersburg, Russia.

[†] On leave from Noncommercial Partnership “Scientific Instruments”, Moscow, Russia.

I. INTRODUCTION

The van der Waals interaction is the well known example of dispersion forces and there is an extensive literature devoted to this subject (see, e.g., monographs [1, 2, 3]). These forces are of quantum origin and they become detectable with a decrease of separation distances between atoms, molecules and macroscopic bodies. Further miniaturization, which is the main tendency of microelectronics, brings more and more attention to the investigation of fine properties of the van der Waals interaction.

The van der Waals force between an atom (molecule) and a cavity wall has long been investigated. In Ref. [4] its interaction potential was found in the form of $V_3(a) = -C_3/a^3$ in nonrelativistic approximation (a is the separation between an atom and a wall). The coefficient C_3 was calculated and measured for different atoms and wall materials, both metallic [5, 6, 7] and dielectric [8, 9]. The theoretical and experimental results were shown to be in qualitative agreement. More precise measurements were performed in Refs. [10, 11]. Currently the van der Waals interaction attracts considerable interest in connection with experiments on quantum reflection of ultracold atoms on different surfaces [12, 13]. With the increase of separation distances up to hundreds nanometers and more to several micrometers, the relativistic and thermal effects become significant changing the dependence of the van der Waals force on separation. At moderate separations up to $1\ \mu\text{m}$ for atoms described by the static atomic polarizability near a wall made of ideal metal at zero temperature the interaction potential was found by Casimir and Polder [14] in the form $V_4(a) = -C_4/a^4$.

Both the van der Waals and Casimir-Polder interactions are of much importance in connection with the experiments on Bose-Einstein condensation of ultracold atoms confined in a magnetic trap near a surface [15, 16, 17]. They may influence the stability of a condensate and the effective size of the trap [17]. Conversely, the Bose-Einstein condensates can be used as sensors of the van der Waals and Casimir-Polder forces. The presence of these forces leads to the shift of the oscillation frequency of the trapped condensate [18]. Note that in application to ultracold atoms not their temperature but the temperature of the wall is the characteristic parameter of the fluctuating electromagnetic field giving rise to the van der Waals interaction [18, 19].

It is common knowledge that the precision of frequency shift measurements is very high. Interpretation of these measurements requires accurate theoretical results for the van der

Waals and Casimir-Polder interaction beyond the expressions given by the simple asymptotic formulas (in fact coefficients C_3 and C_4 are not constants but depend on both separation distance and temperature, and there is smooth joining between the formulas at some intermediate separations). In the case of the Casimir-Polder forces such results were obtained in Ref. [19] for different atoms near a metal wall with account of finite conductivity of a metal, dynamic atomic polarizability and nonzero temperature. In Ref. [18] the influence of the Casimir-Polder force between Rb atoms and sapphire wall onto the oscillations of a condensate was investigated.

In the present paper we find accurate dependences of the van der Waals atom-wall interaction on the dynamic polarizability of an atom and conductivity properties of wall material. As an example, two different atoms are considered (metastable He^* and Na), and metallic (Au), semiconductor (Si) and dielectric (vitreous SiO_2) walls. All calculations are performed within the separation distances $3 \text{ nm} \leq a \leq 150 \text{ nm}$ (for Au at larger separations the accurate theoretical results for the Casimir-Polder interaction were obtained in Ref. [19]). The theoretical formalism for the exact computation of the van der Waals interaction is given by the Lifshitz formula [20, 21, 22] adapted for the configuration of an atom near a wall.

At small separations, characteristic for the van der Waals force, it is necessary to use the complete optical tabulated data for the complex index of refraction in order to find the behavior of the dielectric permittivity along the imaginary frequency axis (at separations $a \geq 150 \text{ nm}$, as was shown in Ref. [19], the dielectric function of the free electron plasma model can be used in the case of an Au wall to find the Casimir-Polder interaction). We compare the results obtained by the use of complete data for the dynamic polarizability of an atom and the ones given by the single-oscillator model. This gave the possibility to obtain more accurate results than in Ref. [23], where the single-oscillator model was used for a hydrogen atom near a silver wall, and also to determine the accuracy of the single-oscillator approximation for the dynamic polarizability in the calculations of the van der Waals interaction. It is shown that to calculate the atom-wall van der Waals interaction with an error less than 1% at a separation of several nanometers both the complete optical tabulated data of the wall material and the accurate atomic dynamic polarizability should be used.

The paper is organized as follows. In Sec. II we briefly present the main formulas and notations for the van der Waals interaction between an atom and a cavity wall. Sec. III

contains the accurate theoretical results for van der Waals interaction of He* and Na atoms with an Au wall. In Sec. IV the analogical results are presented for semiconductor (Si) and dielectric (vitreous SiO₂) walls. Sec. V contains our conclusions and discussion.

II. LIFSHITZ FORMULA FOR VAN DER WAALS ATOM-WALL INTERACTION

The Lifshitz formula for the free energy of atom-wall interaction (wall is at a temperature T at thermal equilibrium) can be presented in the form [19, 22]

$$\mathcal{F}(a, T) = -k_B T \sum_{l=0}^{\infty} \left(1 - \frac{1}{2} \delta_{l0}\right) \alpha(i\xi_l) \int_0^{\infty} k_{\perp} dk_{\perp} q_l e^{-2aq_l} \quad (1)$$

$$\times \left\{ 2r_{\parallel}(\xi_l, k_{\perp}) + \frac{\xi_l^2}{q_l^2 c^2} [r_{\perp}(\xi_l, k_{\perp}) - r_{\parallel}(\xi_l, k_{\perp})] \right\},$$

where $\alpha(\omega)$ is the atomic dynamic polarizability, k_B is the Boltzmann constant, $\xi_l = 2\pi k_B T l / \hbar$ are the Matsubara frequencies, $l = 0, 1, 2, \dots$, δ_{lk} is the Kronecker symbol, and the reflection coefficients for two independent polarizations of the electromagnetic field are

$$r_{\parallel}(\xi_l, k_{\perp}) = \frac{\varepsilon_l q_l - k_l}{\varepsilon_l q_l + k_l},$$

$$r_{\perp}(\xi_l, k_{\perp}) = \frac{k_l - q_l}{k_l + q_l}. \quad (2)$$

In Eqs. (1) and (2) the notations

$$q_l = \sqrt{k_{\perp}^2 + \frac{\xi_l^2}{c^2}}, \quad k_l = \sqrt{k_{\perp}^2 + \varepsilon_l \frac{\xi_l^2}{c^2}} \quad (3)$$

are also introduced, where $\varepsilon_l = \varepsilon(i\xi_l)$ is the dielectric permittivity computed at the imaginary Matsubara frequencies, k_{\perp} is the wave vector in the plane of the wall.

We will apply Eq. (1) in the separation region $3 \text{ nm} \leq a \leq 150 \text{ nm}$ which corresponds to the van der Waals interaction (near the left-hand side of the interval) and transition domain to the Casimir-Polder interaction. In fact, in this region at room temperature $T = 300 \text{ K}$ the temperature effect is negligible. For the sake of convenience in numerical computations we, however, do not make the approximate change of the discrete summation for integration over continuous frequencies and use the original exact Eq. (1).

For further application in computations, we introduce the dimensionless variables

$$y = 2aq_l, \quad \zeta_l = \frac{2a\xi_l}{c} \equiv \frac{\xi_l}{\omega_c}, \quad (4)$$

where $\omega_c \equiv \omega_c(a) = c/(2a)$ is the characteristic frequency of the van der Waals interaction.

Separating the zero-frequency term, Eq. (1) can be represented in the form

$$\mathcal{F} = -\frac{C_3(a, T)}{a^3}, \quad (5)$$

$$C_3(a, T) = \frac{k_B T}{8} \left\{ 2\alpha(0) \frac{\varepsilon(i0) - 1}{\varepsilon(i0) + 1} + \sum_{l=1}^{\infty} \alpha(i\zeta_l \omega_c) \right. \\ \left. \times \int_{\zeta_l}^{\infty} dy e^{-y} \left[2y^2 r_{\parallel}(\zeta_l, y) + \zeta_l^2 [r_{\perp}(\zeta_l, y) - r_{\parallel}(\zeta_l, y)] \right] \right\}.$$

Note that for metal $[\varepsilon(i0) - 1]/[\varepsilon(i0) + 1] = 1$, whereas for dielectrics and semiconductors this ratio is equal to $(\varepsilon_0 - 1)/(\varepsilon_0 + 1)$, where ε_0 is the static dielectric permittivity.

In terms of the new variables the reflection coefficients (2) are

$$r_{\parallel}(\zeta_l, y) = \frac{\varepsilon_l y - \sqrt{y^2 + \zeta_l^2 (\varepsilon_l - 1)}}{\varepsilon_l y + \sqrt{y^2 + \zeta_l^2 (\varepsilon_l - 1)}}, \\ r_{\perp}(\zeta_l, y) = \frac{\sqrt{y^2 + \zeta_l^2 (\varepsilon_l - 1)} - y}{\sqrt{y^2 + \zeta_l^2 (\varepsilon_l - 1)} + y}. \quad (6)$$

In a nonrelativistic limit Eq. (5) leads to

$$C_3(T) = \frac{k_B T}{4} \left[\alpha(0) \frac{\varepsilon(i0) - 1}{\varepsilon(i0) + 1} + 2 \sum_{l=1}^{\infty} \alpha(i\xi_l) \frac{\varepsilon(i\xi_l) - 1}{\varepsilon(i\xi_l) + 1} \right], \quad (7)$$

which gives the usual estimation for the value of the van der Waals constant at the shorter separations. Remind that Eq. (7) practically does not depend on temperature. By using the Abel-Plana formula [24] it can be approximately represented by

$$C_3 \approx \frac{\hbar}{4\pi} \int_0^{\infty} \alpha(i\xi) \frac{\varepsilon(i\xi) - 1}{\varepsilon(i\xi) + 1} d\xi. \quad (8)$$

In the next two sections Eqs. (5)–(7) will be used for accurate calculations of the van der Waals force between different atoms near the surfaces made of metallic, semiconducting and dielectric materials.

III. VAN DER WAALS INTERACTION OF He* AND Na ATOMS WITH GOLD WALL

To calculate the van der Waals free energy of atom-wall interaction one should substitute the values of the dielectric permittivity of the wall material and dynamic polarizability of the atom at imaginary Matsubara frequencies into Eqs. (5) and (6).

We consider the separation distances $a \leq 150$ nm (at larger separations the analytical representation for \mathcal{F} was obtained in Ref. [19] using the plasma model dielectric function and the single oscillator model for the atomic dynamic polarizability; the agreement up to 1% with the results of numerical computations was achieved). As a lower limit of separations under consideration we fix $a = 3$ nm. At smaller separation distances there are additional physical phenomena, connected with the atomic structure of a wall material, which are not taken into account in Eq. (5) but can influence atom-wall interaction. The most important of them are the repulsive exchange potentials with a range of action up to a few angströms, and the spatially nonlocal interaction due to the surface-plasmon charge fluctuations. The latter contributes essentially at separations of the order of $v_F/\omega_p \sim 1$ Å, where v_F is the Fermi velocity and ω_p is the plasma frequency [25]. As was proved in Ref. [25], at much larger separations (in fact, starting from $a \approx 3$ nm) the usual Lifshitz formula, given by Eqs. (1) and (5) is already applicable.

Within the separation region under consideration the characteristic frequency ω_c reaches and even exceeds (at the shorter separations) the plasma frequency (for Au we use $\omega_p = 1.37 \times 10^{16}$ rad/s [26]). By this reason in our case the plasma or Drude dielectric functions are not good approximations for the dielectric permittivity in all relevant frequency range and one should use the complete tabulated data for the complex index of refraction for Au to calculate the imaginary part of the dielectric permittivity $\text{Im}\varepsilon(\omega)$ along the real frequency axis. The dielectric permittivity along the imaginary frequency axis is found by means of the dispersion relation [27]

$$\varepsilon(i\xi) = 1 + \frac{2}{\pi} \int_0^\infty d\omega \frac{\omega \text{Im}\varepsilon(\omega)}{\omega^2 + \xi^2}. \quad (9)$$

The available tabulated data for Au extend from 0.125 eV to 10000 eV ($1 \text{ eV} = 1.519 \times 10^{15}$ rad/s). At shorter separations, to obtain the values of the van der Waals free energy correct up to four significant figures, one should find the dielectric permittivity at first 1850 Matsubara frequencies. Near the right border of the separation interval ($a = 150$ nm) it would suffice to use only 60–70 first Matsubara frequencies. In fact, to obtain ε by Eq. (9) with sufficient precision one should extend the available tabulated data for the region $\omega < 0.125$ eV. This is conventionally done with the help of the imaginary part of the Drude dielectric function

$$\varepsilon(\omega) = 1 - \frac{\omega_p^2}{\omega(\omega + i\gamma)}, \quad (10)$$

where $\gamma = 0.035$ eV is the relaxation frequency. It should be reminded also that Eqs. (1), (2), (10) are free from contradiction with the Nernst heat theorem which arise when the Drude dielectric function is substituted into the Lifshitz formula at nonzero temperature in the configuration of two parallel plates made of real metal (see Refs. [28, 29] for more details).

The computational results for Au are presented in Fig. 1 where $\log_{10} \varepsilon(i\xi)$ is plotted as a function of $\log_{10} \xi$ starting from the first Matsubara frequency (at $T = 300$ K one has $\xi_1 \approx 2.47 \times 10^{14}$ rad/s and $\log_{10} \xi_1 \approx 14.4$).

Other data to be substituted into Eq. (5) are the values of the atomic dynamic polarizability at imaginary Matsubara frequencies. The accurate data (having a relative error of about 10^{-6}) were taken from Ref. [30] for the atoms of metastable He* and from Ref. [31] for Na (see also the graphical representation in Fig. 3 of Ref. [19]). It is interesting to compare the values of $C_3(a, T)$ obtained by the use of the highly accurate data for the atomic dynamic polarizability and in the framework of the single oscillator model

$$\alpha(i\zeta\omega_c) = \frac{\alpha(0)}{1 + \frac{\omega_c^2 \zeta^2}{\omega_0^2}}, \quad (11)$$

where for He* it holds $\alpha(0) = 315.63$ a.u., $\omega_0 = 1.18$ eV [32] and for Na it holds $\alpha(0) = 162.68$ a.u., $\omega_0 = 1.55$ eV [33] (1 a.u. of polarizability is equal to 1.48×10^{-31} m³).

The computational results for the van der Waals coefficient C_3 in the case of Au wall versus separation are represented in Fig. 2 for metastable He* (a) and Na (b) by solid lines. These lines are obtained by the use of the optical tabulated data for $\text{Im}\varepsilon$ and accurate atomic dynamic polarizability. In the same figure the long-dashed lines show the results obtained with the same data for $\text{Im}\varepsilon$ but with a single oscillator model (11) for the atomic dynamic polarizability. The short-dashed lines illustrate the dependence of C_3 on a in the case of a wall made of ideal metal but with the accurate atomic dynamic polarizability.

As is seen from Fig. 2, the account of the realistic properties of a wall metal is important at all separations under consideration. At the shortest separation $a = 3$ nm the result for an ideal metal differs from the accurate result given by the solid line by about 16% for He* and by 28% for Na. These strong deviations only slightly decrease with the increase of separation.

A few calculated results for the values of C_3 are presented in Table I at $T = 300$ K for different separations indicated in the first column. In columns 2 and 3 the values of C_3 for

He* atom are computed for ideal metal and by the use of the optical tabulated data for $\text{Im}\epsilon$, respectively, and in both cases with an accurate atomic polarizability. In column 4 the optical tabulated data for $\text{Im}\epsilon$ were used in combination with the single oscillator model for the atomic polarizability of He*. In column 5 the plasma model dielectric function was used in calculations together with an accurate atomic polarizability of He*. In columns 6–9 the calculational results for a Na atom are presented in the same order.

As is seen from Fig. 2 and Table I (columns 3 and 4), the use of the accurate data for the atomic dynamic polarizability (if to compare with the single oscillator model) is of most importance at the shortest separations. Thus, at $a = 3$ nm the relative error of C_3 given by the single oscillator model is 4.4% for He* and 2.2% for Na. At $a = 15$ nm the single oscillator model becomes more precise. For He* it leads to only 3.3%, and for Na to 1.6% errors.

It is interesting to compare the calculated results obtained by the use of the complete tabulated data for $\text{Im}\epsilon$ of Au and by the plasma model dielectric function [Eq. (10) with $\gamma = 0$]. From columns 3 and 5 of Table I for He*, and 7 and 9 for Na one can conclude that the error, given by the plasma model, decreases from 6.3% for He* and 10% for Na at $a = 3$ nm to 0.8% for He* and 1% for Na at $a = 150$ nm. This illustrates the smooth joining of our present results for the van der Waals interaction obtained by the use of the optical tabulated data for Au with the analytical results of Ref. [19] for the Casimir-Polder interaction found by the application of the plasma model.

The nonrelativistic asymptotic values of C_3 can be calculated by the immediate use of Eqs. (7) and (9) combined with the optical tabulated data for $\text{Im}\epsilon$ and the accurate atomic polarizability. This leads to the results $C_3 \approx 1.61$ a.u. for He* and $C_3 \approx 1.37$ a.u. for Na in rather good agreement with the data of columns 3 and 7 of Table I computed at the shortest separation $a = 3$ nm. Note, however, that the asymptotic values, achieved at separations $a < 3$ nm, may be already outside of the application region of the used theoretical approach (see discussion in the beginning of this section).

As was shown in Ref. [19], the account of the atomic dynamic polarizability strongly affects the value of the Casimir-Polder interaction if to compare with the original result [14] obtained in the static approximation. We emphasize that in the case of the van der Waals interaction the influence of dynamic effects is even greater than in the Casimir-Polder case. Thus, if we restrict ourselves by only static polarizability of He* atom, the values of

C_3 are found to be 11.6 and 1.64 times greater than those given in column 3 of Table I at separations $a = 3$ nm and $a = 150$ nm, respectively.

IV. VAN DER WAALS INTERACTION OF He* AND Na ATOMS WITH SEMICONDUCTOR AND DIELECTRIC WALLS

In this section we apply the formalism of Sec. II to find the accurate separation dependences of the van der Waals interaction between He* and Na atoms and Si or vitreous SiO₂ wall. The chosen separation interval $3 \text{ nm} \leq a \leq 150 \text{ nm}$ is the same as in Sec. III. In the case of dielectric and semiconductor surfaces there are additional interactions due to the charged dangling bonds at separations 1–1.5 nm (see, e.g., Ref. [34]). This is a further factor restricting the application of the conventional theory of van der Waals forces at very short distances.

The tabulated data for the complex refraction index of Si extend from 0.00496 eV to 2000 eV [26]. This permits not to use any extension of data to smaller frequencies when using Eq. (9) in order to find the dielectric permittivity at all contributing imaginary Matsubara frequencies. The computational results for Si are presented in Fig. 3a where $\varepsilon(i\xi)$ is plotted as a function of $\log_{10} \xi$ (ξ is measured in rad/s). The static dielectric permittivity of Si is equal to $\varepsilon_0 = 11.66$.

Substituting the obtained results for $\varepsilon(i\xi)$ and also the data for the atomic dynamic polarizability of He* and Na (the same as in Sec. III) into Eqs. (5) and (6), one finds the dependences of the van der Waals parameter C_3 on separation. The results are shown in Fig. 4a (for He*) and Fig. 4b (for Na). The solid lines are obtained by the use of the accurate atomic dynamic polarizabilities, and the long-dashed lines by using the single oscillator model given by Eq. (11). The short-dashed lines are obtained with the accurate dynamic polarizability but on the assumption that the dielectric permittivity does not depend on frequency and is equal to its static value. At the shortest separation $a = 3$ nm the error in C_3 due to the use of the static dielectric permittivity is approximately 13% for He* and 24% for Na.

In Table II a few calculated values of C_3 at $T = 300$ K are presented at separations listed in column 1. In columns 2 and 3 the values of C_3 for He* are computed by the use of a static dielectric permittivity and optical tabulated data for $\text{Im}\varepsilon$, respectively, and in both cases

with the accurate atomic dynamic polarizability. In column 4 the data for $\text{Im}\varepsilon$ were used in combination with the single oscillator model for He^* dynamic polarizability. In columns 5–7 the same results for a Na atom are presented.

Table II and Fig. 4 permit to follow the influence of atomic and semiconductor characteristics onto the van der Waals force. Thus, comparing columns 3 and 4 we notice that the use of the single oscillator model leads to 4.4% error at $a = 3$ nm and 3.1% error at $a = 15$ nm for the atom of metastable He^* . For the atom of Na these errors are 1.8% and 1%, respectively. With the increase of separation distance up to 150 nm the errors given by the single oscillator model decrease down to 0.4% for He^* and practically to zero for Na. This confirms that at larger separations the single oscillator model is quite sufficient for calculations of the van der Waals interactions with errors below 1%.

Now let us consider the case of a dielectric wall (vitreous SiO_2). The tabulated data for the complex refraction index of SiO_2 extend from 0.0025 eV to 2000 eV [26]. This is also quite sufficient to calculate the dielectric permittivity at all contributing Matsubara frequencies by Eq. (9) with no use of any extension of data. The dependence of $\varepsilon(i\xi)$ as a function of $\log_{10} \xi$ for SiO_2 is shown in Fig. 3b. The static dielectric permittivity of SiO_2 is equal to $\varepsilon_0 = 4.88$.

The obtained results for $\varepsilon(i\xi)$ and the data for the atomic dynamic polarizability of He^* and Na are substituted into Eqs. (5) and (6). The resulting dependences of C_3 on separation are shown in Fig. 5a (for He^*) and Fig. 5b (for Na). As in Fig. 4, the solid lines are related to the use of the accurate dynamic polarizabilities, the long-dashed lines to the single oscillator model, and the short-dashed lines to the use of the static dielectric permittivity and an accurate dynamic polarizability.

Table III, containing a few calculated results, is organized in the same way as Table II related to the case of a semiconductor wall. It permits to find errors resulting from the use of the static dielectric permittivity instead of the accurate dependence of $\varepsilon(i\xi)$ on frequency, and a single oscillator model instead of an accurate dynamic polarizability for the atom near the dielectric wall. Thus, at $a = 3$ nm the use of the static dielectric permittivity instead of the optical tabulated data leads to 78% error in the value of the van der Waals coefficient C_3 for He^* and to 95% error for Na. These errors decrease to 2.1% and 6.9%, respectively, if one uses the dielectric permittivity $\tilde{\varepsilon} \approx 2.13$ corresponding not to the zero frequency but to the frequency region of visible light. With the use of $\tilde{\varepsilon}$ the largest errors in the value

of C_3 are achieved, however, not at the shortest separation but at the largest separation considered here $a = 150$ nm (15% for He* atom and 12.7% for Na atom). At this separation the use of the static dielectric permittivity ε_0 leads to 56.6% error (for He*) and 62% error (for Na).

By the comparison of columns 3 and 4 in Table III we conclude that at a separation $a = 3$ nm the use of the single oscillator model results in 5% error for He* atom and in 3% error for Na atom. At $a = 15$ nm the corresponding errors are 3.6% and 1.2%, respectively. At a separation $a = 150$ nm the errors due to the use of the single oscillator model are 0.6% for He* atom and practically zero for Na atom, i.e., the single oscillator model is sufficient.

V. CONCLUSIONS AND DISCUSSION

In the foregoing we have performed accurate calculations of the parameter C_3 describing the van der Waals atom-wall interaction for the atoms of metastable He* and Na near metallic, semiconductor and dielectric walls. The separation region from 3 nm to 150 nm was considered covering the proper nonrelativistic van der Waals interaction and some part of the transition region to the relativistic Casimir-Polder interaction. At $a = 150$ nm the smooth joining of the obtained results with the calculations of Ref. [19] for the Casimir-Polder case was followed.

It was shown that qualitatively the cases of an atom near metallic, semiconductor and dielectric walls are very similar. The use of approximations of the ideal metal or the static dielectric permittivity leads to the errors in the value of C_3 of about (13–28)% at the shortest separation depending on the wall material and the type of atoms. This error slowly decreases with the increase of separation remaining rather large in the case of metallic wall. The more adequate (for metals) plasma model dielectric function results in (6–10)% errors at the shortest separation.

We have compared the results for C_3 obtained by the use of the accurate atomic dynamic polarizability with those obtained from the single oscillator model. At the shortest separation the single oscillator model leads to errors of about (1.8–4.4)% in the values of C_3 . These errors quickly decrease with the increase of separation.

The magnitude of the error, given by one or another approximation used, depends qualitatively on the type of the atom. By way of example, for Na atom the use of a single

oscillator model leads to less errors than for He* independently of wall material.

The performed investigation permits to make a conclusion that the accurate calculations of the van der Waals atom-wall interaction at short separations with the error no larger than 1% require the use of both complete optical tabulated data of wall material and accurate dynamic polarizability of an atom. This is distinct from the case of the Casimir-Polder interaction with a metallic wall which can be described with no more than 1% error using the plasma model dielectric function of a wall material and the single oscillator model for the dynamic polarizability of an atom.

The obtained results can be used for theoretical interpretation of the experiments on quantum reflection and Bose-Einstein condensation of ultracold atoms on (near) surfaces of different nature, and also in investigation of other physical, chemical and biological processes, where the precise information on the van der Waals and Casimir-Polder forces is needed.

Acknowledgments

The authors are grateful to J. F. Babb for stimulating discussions and for giving accurate data on the atomic dynamic polarizability of He* and Na. We gratefully acknowledge FAPERJ (Processes E-26/170.132 and 170.409/2004) for financial support. G.L.K. and V.M.M. were partially supported by Finep.

-
- [1] J. Israelachvili, *Intermolecular and Surface Forces* (Academic Press, San Diego, 1992).
 - [2] J. Mahanty and B. W. Ninham, *Dispersion Forces* (Academic Press, New York, 1976).
 - [3] Yu. S. Barash, *van der Waals Forces* (Nauka, Moscow, 1988), in Russian.
 - [4] J. E. Lennard-Jones, *Trans. Faraday Soc.* **28**, 333 (1932).
 - [5] A. Shih, D. Raskin, and P. Kusch, *Phys. Rev. A* **9**, 652 (1974).
 - [6] A. Shih, *Phys. Rev. A* **9**, 1507 (1974).
 - [7] A. Shih and V. A. Parsegian, *Phys. Rev. A* **12**, 835 (1975).
 - [8] E. Zaremba and W. Kohn, *Phys. Rev. A* **13**, 2270 (1976).
 - [9] G. Vidali and M. W. Cole, *Surf. Sci.* **110**, 10 (1981).
 - [10] M. Oria, M. Chrevrollier, D. Bloch, M. Fichet, and M. Ducloy, *Europhys. Lett.* **14**, 527 (1991).

- [11] V. Sandoghdar, C. I. Sukenik, and E. A. Hinds, *Phys. Rev. Lett.* **68**, 3432 (1992).
- [12] F. Shimizu, *Phys. Rev. Lett.* **86**, 987 (2001).
- [13] V. Druzhinina and M. DeKieviet, *Phys. Rev. Lett.* **91**, 193202 (2003).
- [14] H. B. G. Casimir and D. Polder, *Phys. Rev.* **73**, 360 (1948).
- [15] D. M. Harber, J. M. McGuirk, J. M. Obrecht, and E. A. Cornell, *J. Low Temp. Phys.* **133**, 229 (2003).
- [16] A. E. Leanhardt, Y. Shin, A. P. Chikkatur, D. Kielpinski, W. Ketterle, and D. E. Pritchard, *Phys. Rev. Lett.* **90**, 100404 (2003).
- [17] Y. Lin, I. Teper, C. Chin, and V. Vuletić, *Phys. Rev. Lett.* **92**, 050404 (2004).
- [18] M. Antezza, L. P. Pitaevskii, and S. Stringari, *Phys. Rev. A* **70**, 053619 (2004).
- [19] J. F. Babb, G. L. Klimchitskaya, and V. M. Mostepanenko, *Phys. Rev. A* **70**, N3 (2004); e-print quant-ph/0405163.
- [20] E. M. Lifshitz, *Zh. Eksp. Teor. Fiz.* **29**, 94 (1956) [*Sov. Phys. JETP* **2**, 73 (1956)].
- [21] I. E. Dzyaloshinskii, E. M. Lifshitz, and L. P. Pitaevskii, *Usp. Fiz. Nauk* **73**, 381 (1961) [*Sov. Phys. Usp. (USA)* **4**, 153 (1961)].
- [22] E. M. Lifshitz and L. P. Pitaevskii, *Statistical Physics*, Part. II (Pergamon Press, Oxford, 1980).
- [23] M. Boström and B. E. Sernelius, *Phys. Rev. A* **61**, 052703 (2000).
- [24] V. M. Mostepanenko and N. N. Trunov, *The Casimir Effect and its Applications* (Clarendon Press, Oxford, 1997).
- [25] J. Heinrichs, *Phys. Rev. B* **11**, 3625 (1975).
- [26] *Handbook of Optical Constants of Solids*, ed. E. D. Palik (Academic, New York, 1985).
- [27] L. D. Landau, E. M. Lifshitz and L. P. Pitaevskii, *Electrodynamics of Continuous Media* (Pergamon Press, Oxford, 1984).
- [28] B. Geyer, G. L. Klimchitskaya, and V. M. Mostepanenko, *Phys. Rev. A* **67**, 062102 (2003).
- [29] V. B. Bezerra, G. L. Klimchitskaya, V. M. Mostepanenko, and C. Romero, *Phys. Rev. A* **69**, 022119 (2004).
- [30] Z.-C. Yan and J. F. Babb, *Phys. Rev. A* **58** 1247 (1998).
- [31] P. Kharchenko, J. F. Babb, and A. Dalgarno, *Phys. Rev. A* **55**, 3566 (1997).
- [32] R. Brühl, P. Fouquet, R. E. Grisenti, J. P. Toennies, G. C. Hegerfeldt, T. Köhler, M. Stoll, and C. Walter, *Europhys. Lett.* **59**, 357 (2002).

- [33] A. Derevianko, W. R. Johnson, M. S. Safronova, and J. F. Babb, *Phys. Rev. Lett.* **82**, 3589 (1999).
- [34] V. N. Filipovich, G. L. Klimchitskaya, and B. F. Shchegolev, *J. Phys. C* **16**, 6561 (1983).

Figures

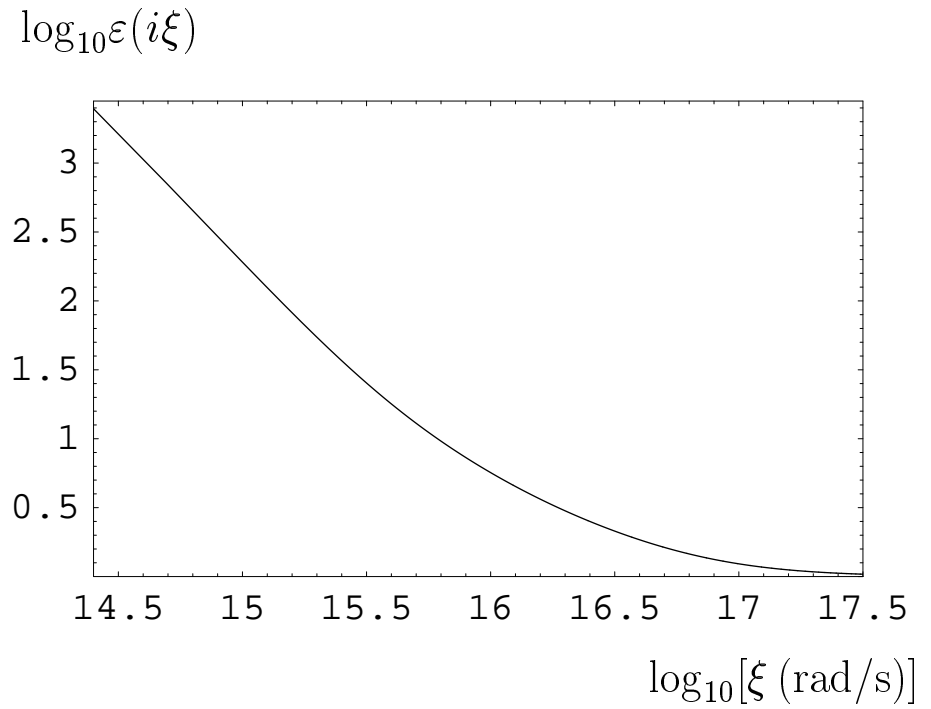


FIG. 1: Logarithm of the dielectric permittivity of Au along the imaginary axis as a function of the logarithm of frequency.

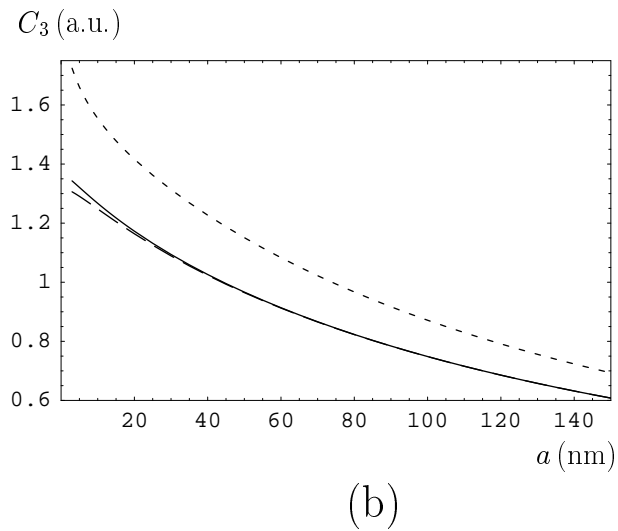
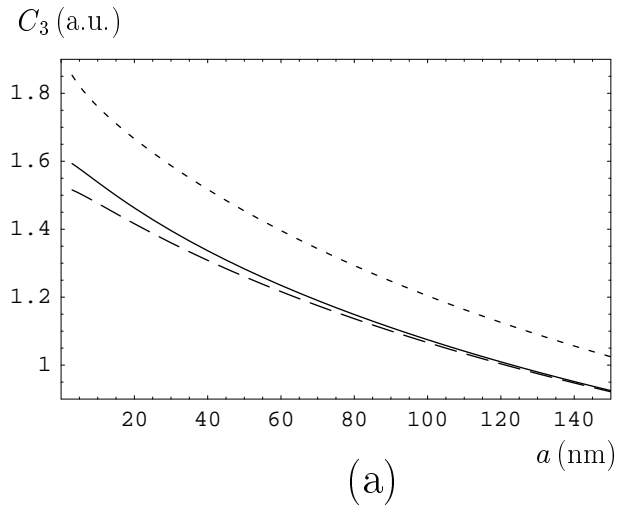


FIG. 2: Dependence of the van der Waals coefficient C_3 on separation for metastable He^* (a) and Na (b) atoms near Au wall calculated by the use of the complete tabulated data of Au and the accurate atomic dynamic polarizabilities (solid lines) or by the single oscillator model (long-dashed lines). The short-dashed lines are calculated for the ideal metal with the accurate dynamic polarizability of the atoms.

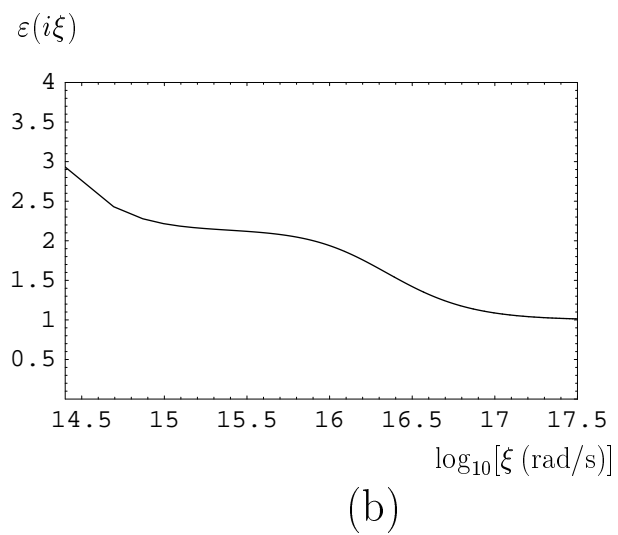
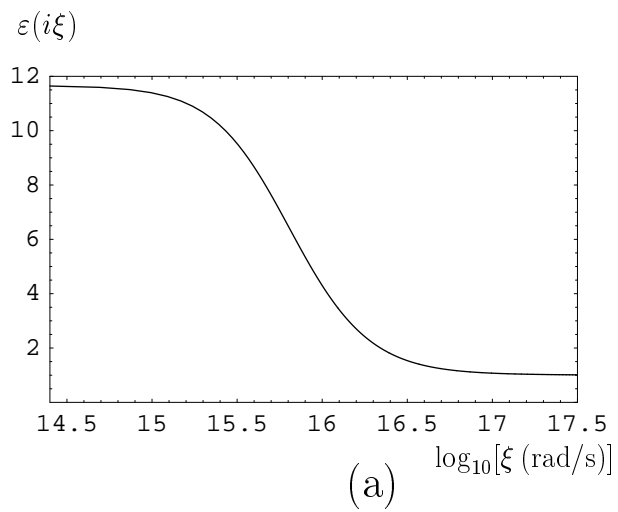


FIG. 3: Dielectric permittivity of Si (a) and SiO₂ (b) along the imaginary axis as a function of the logarithm of frequency.

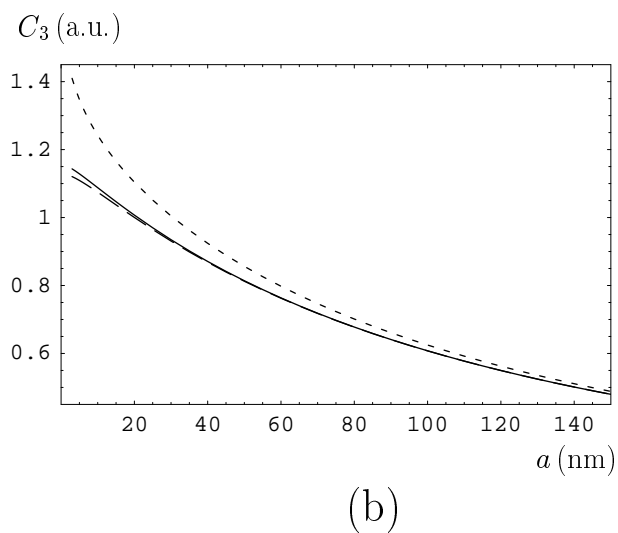
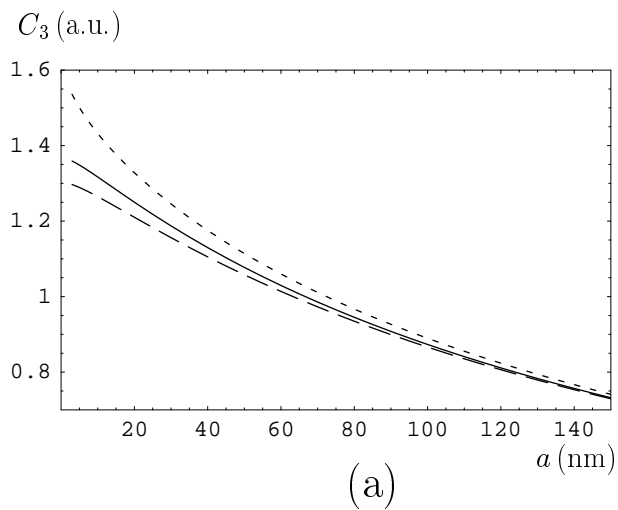


FIG. 4: Dependence of the van der Waals coefficient C_3 on separation for metastable He^* (a) and Na (b) atoms near Si wall calculated by the use of the complete tabulated data of Si with the accurate atomic dynamic polarizabilities (solid lines) and by the single oscillator model (long-dashed lines). The short-dashed lines are calculated for semiconductor, described by the static dielectric permittivity, and by the accurate dynamic polarizability of the atoms.

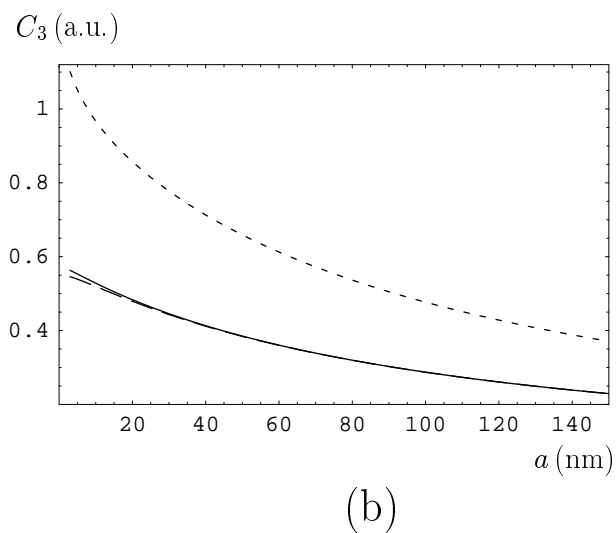
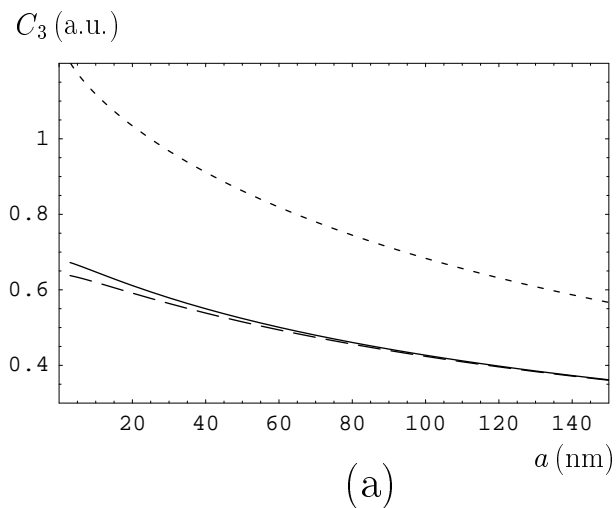


FIG. 5: Dependence of the van der Waals coefficient C_3 on separation for metastable He^* (a) and Na (b) atoms near SiO_2 wall calculated by the use of the complete tabulated data of SiO_2 with the accurate atomic dynamic polarizabilities (solid lines) and by the single oscillator model (long-dashed lines). The short-dashed lines are calculated for dielectric, described by the static dielectric permittivity, and by the accurate dynamic polarizability of the atoms.

Tables

TABLE I: Values of the coefficient C_3 of the van der Waals atom-wall interaction at different separations computed for the ideal metal (a) and for real metal (Au) described by the optical tabulated data (b), and the accurate atomic dynamic polarizabilities; in column (c) real metal is described by the optical tabulated data and the dynamic polarizability of an atom is given by the single oscillator model; in column (d) real metal is described by the plasma model and the dynamic polarizability of an atom is accurate.

a (nm)	Metastable He* near Au wall				Na near Au wall			
	(a)	(b)	(c)	(d)	(a)	(b)	(c)	(d)
3	1.85	1.59	1.52	1.49	1.72	1.34	1.31	1.20
5	1.82	1.58	1.51	1.48	1.66	1.32	1.29	1.19
10	1.76	1.54	1.48	1.46	1.55	1.27	1.25	1.16
15	1.71	1.50	1.45	1.43	1.48	1.22	1.20	1.13
20	1.67	1.46	1.42	1.40	1.42	1.17	1.16	1.10
25	1.62	1.43	1.39	1.38	1.36	1.13	1.12	1.07
50	1.45	1.28	1.26	1.25	1.15	0.967	0.965	0.932
75	1.32	1.17	1.16	1.15	0.994	0.844	0.844	0.822
100	1.20	1.08	1.07	1.06	0.871	0.748	0.748	0.734
125	1.11	0.994	0.989	0.985	0.773	0.671	0.671	0.662
150	1.02	0.925	0.922	0.918	0.693	0.608	0.608	0.601

TABLE II: Values of the coefficient C_3 of the van der Waals atom-wall interaction at different separations computed for the semiconductor (Si) described by the static dielectric permittivity (a) and by the optical tabulated data (b), and the accurate atomic dynamic polarizabilities; in column (c) semiconductor is described by the optical tabulated data and the dynamic polarizability of an atom is given by the single oscillator model.

a (nm)	Metastable He* near Si wall			Na near Si wall		
	(a)	(b)	(c)	(a)	(b)	(c)
3	1.54	1.36	1.30	1.41	1.14	1.12
5	1.50	1.35	1.29	1.35	1.13	1.11
10	1.43	1.32	1.26	1.24	1.09	1.07
15	1.38	1.28	1.24	1.17	1.05	1.04
20	1.33	1.25	1.21	1.10	1.01	1.00
25	1.28	1.22	1.18	1.05	0.970	0.965
50	1.11	1.08	1.06	0.856	0.814	0.812
75	0.998	0.965	0.954	0.723	0.698	0.697
100	0.890	0.873	0.866	0.625	0.608	0.608
125	0.809	0.797	0.792	0.549	0.537	0.537
150	0.741	0.732	0.729	0.488	0.480	0.480

TABLE III: Values of the coefficient C_3 of the van der Waals atom-wall interaction at different separations computed for the dielectric (vitreous SiO_2) described by the static dielectric permittivity (a) and by the optical tabulated data (b), and the accurate atomic dynamic polarizabilities; in column (c) semiconductor is described by the optical tabulated data and the dynamic polarizability of an atom is given by the single oscillator model.

a (nm)	Metastable He^* near SiO_2 wall			Na near SiO_2 wall		
	(a)	(b)	(c)	(a)	(b)	(c)
3	1.20	0.672	0.638	1.10	0.563	0.546
5	1.17	0.666	0.633	1.05	0.553	0.539
10	1.12	0.647	0.620	0.967	0.528	0.519
15	1.07	0.629	0.606	0.906	0.505	0.499
20	1.03	0.611	0.591	0.857	0.484	0.479
25	0.999	0.595	0.577	0.815	0.464	0.461
50	0.862	0.524	0.515	0.659	0.385	0.384
75	0.762	0.470	0.465	0.554	0.329	0.329
100	0.684	0.427	0.424	0.477	0.287	0.287
125	0.620	0.391	0.390	0.418	0.255	0.255
150	0.567	0.362	0.360	0.371	0.229	0.229